2014 14th IEEE-RAS International Conference on
Humanoid Robots (Humanoids)
November 18-20, 2014. Madrid, Spain

Humanoid Locomotion on Uneven Terrain Using the Time-Varying Divergent Component of Motion

Michael A. Hopkins †, Dennis W. Hong ‡, and Alexander Leonessa †*

***Abstract*— This paper presents a framework for dynamic humanoid locomotion on uneven terrain using a novel time-varying extension to the Divergent Component of Motion (DCM). By varying the natural frequency of the DCM, we are able to achieve generic CoM height trajectories during stepping. The proposed planning algorithm computes admissible DCM reference trajectories given desired ZMP plans for single and double support. This is accomplished using reverse-time integration of the discretized DCM dynamics over a finite time horizon. To account for discontinuities during replanning, linear Model Predictive Control (MPC) is implemented over a short preview window. DCM tracking control is achieved using a time-varying proportional-integral controller based on the Virtual Repellent Point (VRP). The effectiveness of the combined approach is verified in simulation using a 30-DoF model of THOR, a compliant torque-controlled humanoid.**

I. Introduction

After decades of research into legged robots, humanoid locomotion controllers are still unable to match the grace and robustness of biological systems. The problem is complicated by the underactuated and nonlinear nature of the associated multibody dynamics. The dynamic planning problem typically requires the generation of centroidal reference trajectories that can be realized using admissible contact forces given mode-dependent contact constraints. To achieve real-time performance, many authors introduce simplifying assumptions which limit locomotion to flat terrain or impose certain restrictions on the vertical center of mass (CoM) or angular momentum trajectories.

A common approach in the walking literature is to generate reference CoM trajectories from admissible Zero-Moment Point (ZMP) trajectories in order to satisfy no-tipping conditions on the support feet. In [1] Kajita proposed a CoM pattern generator based on the analytic solution to the linear inverted pendulum (LIPM) dynamics. In [2] the authors introduced a preview controller to minimize ZMP tracking error by optimizing the CoM jerk. In [3] Wieber proposed a Model Predictive Control (MPC) approach for ZMP tracking using a linearly constrained quadratic program. Although these approaches are based on the LIPM dynamics, some authors have incorporated desired CoM height and angular momentum trajectories using time-varying LQR solutions [4] [5].

The Capture Point (CP) [6] and Divergent Component of Motion (DCM) [7] are equivalent transformations of the CoM state that encode the unstable dynamics of the linear inverted pendulum. By definition, the CoM can be indirectly stabilized by tracking an appropriate CP trajectory. In [8] Englsberger proposed a recursive algorithm to compute CP trajectories for dynamic walking given desired ZMP waypoints, and in [9] this work was extended to three-dimensional DCM trajectories to enable locomotion on uneven terrain. In [10] Morisawa incorporated integral action into the CP controller to eliminate steady-state errors, and in [11] Englsberger introduced a ZMP-based CP tracking controller to compensate for time-varying vertical CoM dynamics and horizontal angular momentum rates of change during stepping. Because these methods assume a constant natural frequency of the LIPM for trajectory planning, the ZMP can deviate from the desired reference when the vertical CoM dynamics do not match the time-invariant LIPM dynamics.

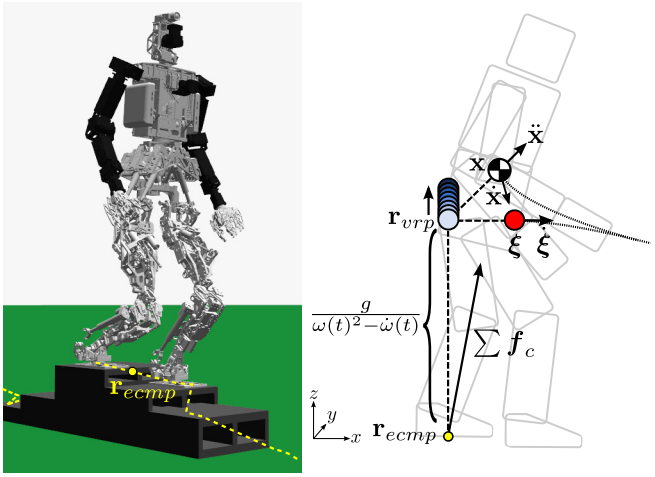

Fig. 1. Left: THOR walking on uneven terrain in simulation. Right: Time-varying Divergent Component of Motion (DCM) dynamics.

This paper introduces a dynamic planning and control approach for humanoid robots using a novel time-varying extension to the DCM. By modifying the definition of the time-varying natural frequency, we derive simple first-order dynamics for the DCM in terms of the Virtual Repellent Point (VRP) introduced in [9]. Using this framework, we present a method to plan DCM reference trajectories for dynamic walking on uneven terrain given generic vertical CoM and ZMP trajectories. This is accomplished using reverse-time integration of the discretized DCM dynamics over a finite time horizon. To account for discontinuities during replanning, linear Model Predictive Control (MPC) is implemented over a short preview window. The effectiveness

†M. A. Hopkins and A. Leonessa are with the Terrestrial Robotics, Engineering & Controls Lab at Virginia Tech. (e-mail: michael.hopkins@vt.edu)
‡D. W. Hong is with the Robotics and Mechanisms Laboratory at UCLA.
*This material is based upon work supported by (while serving at) the National Science Foundation.

of the combined approach is verified through experiments using a simulated 30-DoF model of the THOR humanoid shown in Fig. 1. Although we focus on trajectory generation for the three-dimensional DCM, the proposed algorithms can also be applied to two-dimensional CP planning and control.

II. Divergent Component of Motion

The Divergent Component of Motion (DCM) is a linear transformation of the center of mass (CoM) state used to separate the second-order CoM dynamics into stable and unstable first-order components [7]. In [9] the authors introduced a three-dimensional extension of the DCM defined by

$$\boldsymbol{\xi} = \mathbf{x} + \frac{1}{\omega_0}\dot{\mathbf{x}}, \tag{1}$$

where $\mathbf{x} = [\, x_{com},\ y_{com},\ z_{com}\,]^T$ is the CoM position, $\dot{\mathbf{x}}$ is the CoM velocity and $\omega_0 = \sqrt{\frac{g}{\Delta z_{com}}}$ is the natural frequency of the linear inverted pendulum [1] given a nominal CoM height, Δz_{com}.

The unstable first-order DCM dynamics are given by

$$\dot{\boldsymbol{\xi}} = \omega_0 \left(\boldsymbol{\xi} - \mathbf{r}_{vrp}\right), \tag{2}$$

where $\mathbf{r}_{vrp}$ represents the Virtual Repellent Point (VRP) [9]. Assuming $\omega_0 > 0$, this system has a single pole in the right-half plane. The DCM is repelled away from the VRP at a rate proportional to its distance. This unstable equilibrium point is defined as

$$\mathbf{r}_{vrp} = \mathbf{r}_{ecmp} + [\, 0,\, 0,\, \Delta z_{com}\,]^T, \tag{3}$$

where

$$\mathbf{r}_{ecmp} = \mathbf{x} - \frac{\sum \mathbf{f}_c}{m\omega_0^2} \tag{4}$$

represents the enhanced Centroidal Moment Pivot (eCMP) [9]. The eCMP encodes the direction and magnitude of all contact forces, $\sum \mathbf{f}_c \in \mathbb{R}^3$, acting on the CoM given the total mass m and CoM position $\mathbf{x}$ [9]. When the eCMP intersects the ground plane it coincides with the canonical CMP ground reference point [12]. For planning purposes the eCMP and CMP are often defined to lie within the base of support as shown in Fig. 1 in order to ensure admissibility of contact forces during stepping [13].

From (1) the stable first-order CoM dynamics are given by

$$\dot{\mathbf{x}} = \omega_0(\boldsymbol{\xi} - \mathbf{x}). \tag{5}$$

By definition, the CoM converges to the DCM with a time constant of $\frac{1}{\omega_0}$. Since the zero dynamics of the DCM transformation are asymptotically stable, the centroidal dynamics can be indirectly stabilized by tracking a desired DCM reference trajectory. This property has been exploited by a number of researchers to develop dynamic walking strategies which do not require direct planning of the CoM trajectory [7] [9] [10] [11].

III. Time-Varying DCM

In this section we adapt the Divergent Component of Motion dynamics to account for a time-varying natural frequency, i.e.

$$\boldsymbol{\xi} = \mathbf{x} + \frac{1}{\omega(t)}\dot{\mathbf{x}}. \tag{6}$$

As discussed in Section IV, this relaxation of the original DCM definition enables improved planning of the vertical CoM trajectory during locomotion. When convenient we will use the notation $\omega := \omega(t)$, omitting the natural frequency's explicit dependence on time.

From (6) the time-varying CoM dynamics are given by

$$\dot{\mathbf{x}} = \omega(\boldsymbol{\xi} - \mathbf{x}). \tag{7}$$

Assuming $\omega(t) > \rho$ for some small positive value ρ, this system can be shown to be asymptotically stable with respect to the DCM equilibrium, noting that for the Lyapunov function $V(\mathbf{x}, t) = \frac{1}{2}\mathbf{x}^T\mathbf{x}$ we have $\dot{V}(\mathbf{x}, t) = -\omega(t)\mathbf{x}^T\mathbf{x} < -\rho\mathbf{x}^T\mathbf{x} < 0$. Differentiating the time-varying DCM definition (6) and substituting the CoM dynamics (7) gives

$$\begin{aligned}
\dot{\boldsymbol{\xi}} &= \dot{\mathbf{x}} - \frac{\dot{\omega}}{\omega^2}\dot{\mathbf{x}} + \frac{1}{\omega}\ddot{\mathbf{x}} \\
&= \left(1 - \frac{\dot{\omega}}{\omega^2}\right)\dot{\mathbf{x}} + \frac{1}{\omega}\ddot{\mathbf{x}} \\
&= \left(\omega - \frac{\dot{\omega}}{\omega}\right)(\boldsymbol{\xi} - \mathbf{x}) + \frac{1}{\omega}\ddot{\mathbf{x}} \\
&= \left(\omega - \frac{\dot{\omega}}{\omega}\right)\left(\boldsymbol{\xi} - \left(\mathbf{x} - \frac{\ddot{\mathbf{x}}}{\omega^2 - \dot{\omega}}\right)\right).
\end{aligned} \tag{8}$$

By redefining the VRP in terms of the CoM position and acceleration, i.e.

$$\mathbf{r}_{vrp} = \mathbf{x} - \frac{\ddot{\mathbf{x}}}{\omega^2 - \dot{\omega}}, \tag{9}$$

the time-varying DCM dynamics can be expressed as

$$\dot{\boldsymbol{\xi}} = \left(\omega - \frac{\dot{\omega}}{\omega}\right)\left(\boldsymbol{\xi} - \mathbf{r}_{vrp}\right). \tag{10}$$

This system is inherently unstable with respect to the VRP given $\omega - \dot{\omega}/\omega > 0$. Similar to the time-invariant case, the CoM dynamics can be indirectly stabilized by tracking a desired DCM reference trajectory using an appropriate control law based on the VRP.

Applying Newton's second law, the CoM acceleration can be expressed as $\ddot{\mathbf{x}} = \frac{1}{m}\sum \mathbf{f}_c - \mathbf{g}$ where $\mathbf{g} = [\, 0,\, 0,\, g\,]^T$ is the gravity vector. Substituting this expression into (9) provides the VRP definition in terms of the eCMP,

$$\mathbf{r}_{vrp} = \mathbf{x} - \frac{\sum \mathbf{f}_c - m\mathbf{g}}{m\left(\omega^2 - \dot{\omega}\right)} = \mathbf{r}_{ecmp} + \frac{\mathbf{g}}{\omega^2 - \dot{\omega}}, \tag{11}$$

where the eCMP is redefined as

$$\mathbf{r}_{ecmp} = \mathbf{x} - \frac{\sum \mathbf{f}_c}{m\left(\omega^2 - \dot{\omega}\right)}. \tag{12}$$

As illustrated in Fig. 1, the vertical VRP-eCMP offset varies over time depending on the natural frequency and its first derivative while the horizontal offset remains zero.

Note that for a constant natural frequency, $\omega(t) = \omega_0$ and $\dot{\omega}(t) = 0$, the time-varying CoM-DCM dynamics and VRP-eCMP definitions are equivalent to the time-invariant equations introduced by Englsberger [9]. Examining the z-axis constraints defined in (9) and (11), $\omega(t)$ can be defined in terms of the vertical CoM and eCMP dynamics using the nonlinear differential equation,

$$\omega^2 - \dot{\omega} = \frac{\ddot{z}_{com}}{z_{com} - z_{vrp}} = \frac{\ddot{z}_{com} + g}{z_{com} - z_{ecmp}}. \qquad (13)$$

Thus, the natural frequency of the time-varying DCM is related to the natural frequency of the LIPM [14] by the expression, $\sqrt{\omega^2 - \dot{\omega}} = \sqrt{\frac{\ddot{z}_{com}+g}{\Delta z_{com}}}$ where $\Delta z_{com} = z_{com} - z_{ecmp}$. Note that this is a significant departure from previous CP and DCM publications which define $\omega = \sqrt{\frac{\ddot{z}_{com}+g}{\Delta z_{com}}}$ [10] [11].

If $\omega = 0$ or $\omega^2 - \dot{\omega} = 0$, the DCM dynamics (10) become uncontrollable. In the first case, the time-varying DCM is undefined, and in the second case the commanded contact forces, $\sum \mathbf{f}_c$, become zero. As a result, it is necessary to enforce the constraints $\omega > \rho$ and $\omega^2 - \dot{\omega} > \beta$ for some small positive values ρ and β. This restricts the application of the time-varying DCM to dynamic behaviors such as walking which do not include a flight state.

IV. Locomotion Planning and Control

In this section we present a novel approach to planning and control for humanoid walking using the time-varying DCM. We will assume that a high level footstep planner provides information regarding the desired inertial foothold poses and step durations over a finite time horizon. Given these constraints, the dynamic planning problem addresses the generation of DCM reference trajectories that can be tracked using admissible contact forces during walking. In the proposed approach, trajectories are generated at the onset of each step given a desired terminal DCM state. The complementary dynamic control problem addresses how to track desired DCM reference trajectories using state feedback.

In [9] and [15] Englsberger et al. propose a method to plan 3D DCM trajectories by computing analytic solutions of the reverse-time DCM dynamics given eCMP reference points which lie in the base of support. In order to achieve smooth eCMP and contact force trajectories during double support, the computed DCM reference trajectories are post-processed using polynomial interpolation of critical waypoints. This approach has proven very versatile, enabling fast trajectory planning for walking over uneven terrain using heel-strike and toe-off [15]. In order to compute closed-form solutions, however, these methods introduce certain restrictions on the generated eCMP trajectories and assume a constant natural frequency of the DCM.

In the proposed approach, we compute discrete reference trajectories for the time-varying DCM using a combination of reverse-time integration and Model Predictive Control. By computing solutions numerically rather than analytically, it is possible to achieve generic eCMP trajectories during double and single support. Additionally, by planning appropriate trajectories for the natural frequency of the time-varying DCM, it is possible to achieve arbitrary kinematically feasible CoM height trajectories while stepping. The approach is summarized by the following steps described in this section.

1) Plan the eCMP trajectory given a desired footstep plan.
2) Plan the ω trajectory given a CoM height trajectory.
3) Plan the DCM trajectory using reverse-time integration and Model Predictive Control given a terminal state.
4) Track the DCM reference trajectory using a proportional-integral controller based on the VRP.

A. Planning the eCMP trajectory

Given a desired footstep plan, we begin by computing a ZMP[1] trajectory which intersects the base of support for each step phase. This ensures that the derived eCMP and DCM reference trajectories will satisfy the ZMP criterion [16] given the commanded contact forces. The proposed approach supports arbitrary ZMP trajectories, enabling flat-footed or heel-toe walking. In the experiments presented in Section V, the ZMP trajectory is defined by piecewise 3rd-order polynomials. During double support, the ZMP moves to the center of the new support foot, and during single support, the ZMP moves to the toe-off position.

It is usually desirable to avoid generating significant angular momentum during walking. As a result, many dynamic planning algorithms assume collocation of the ZMP and CMP, resulting in zero angular momentum rate of change, or torque about the CoM. In this case, it is sufficient to define the eCMP equal to the ZMP over the planned preview window in order to satisfy the ZMP criterion. Alternatively, if the expected CoM height trajectory is known in advance, we can shift the eCMP away from the ZMP in order to achieve nonzero horizontal angular momentum rates of change, i.e.

$$\mathbf{r}_{ecmp} = \mathbf{r}_{zmp} + \frac{1}{m\,(g + \ddot{z}_{com})} \left[\, \tau_y \; -\tau_x \; 0 \,\right]^T. \qquad (14)$$

Here τ_x and τ_y represent the desired horizontal moments about the CoM and $\ddot{z}_{com}$ represents the desired vertical acceleration of the CoM.

B. Planning the ω trajectory

The time-varying DCM dynamics derived in Section III provide a simple framework for planning dynamically feasible DCM trajectories given a non-constant natural frequency. Excluding joint torque and range of motion limitations, any continuously differentiable ω trajectory can be realized subject to the constraints $\omega > \rho$ and $\omega^2 - \dot{\omega} > \beta$ for some small positive values ρ and β. In practice, however, it is often useful to compute an explicit plan for the CoM height when stepping over uneven terrain. In this case, the desired ω trajectory can be derived from a nominal vertical CoM trajectory, $z_{com}(t)$, with uniformly continuous velocity.

Solving (13) for $\dot{\omega}$ yields the nonlinear ω dynamics,

$$\dot{\omega} = \omega^2 - \alpha^2(t), \quad \omega(t_0) = \omega_0, \qquad (15)$$

[1]Note that the three-dimensional ZMP is not well-defined in the walking literature. Here we assume equivalence of the ZMP and center of pressure.

where $\alpha(t)$ is the natural frequency of the LIPM defined by $\sqrt{\frac{\ddot{z}_{com}+g}{z_{com}-z_{ecmp}}}$. Thus, the reverse-time dynamics are given by

$$\dot{\omega}_r = \alpha^2(t_r) - \omega^2, \qquad \omega(t_f) = \omega_f, \tag{16}$$

where $\dot{\omega}_r = -\dot{\omega}$ is the reverse-time derivative of the natural frequency, ω_f is the value of ω at the final time t_f, and $t_r = t_f - (t - t_0)$ is the reverse time variable.

Given $\omega_f > 0$, the reverse-time solution, $\omega(t_r)$, converges to $\alpha(t_r)$ as $t_r \to -\infty$ and $\dot{\alpha}(t_r) \to 0$. Furthermore, if $\omega_f > \rho$ and $\alpha(t_r) > \rho \ \forall t_r < t_f$ for some small positive value ρ, then $\omega(t_r) > \rho \ \forall t_r < t_f$. To see this note that if $\alpha^2(t_r) > \omega^2(t_r) > \rho^2$ then $\dot{\omega}_r > 0$. Referring back to the forward-time dynamics, these conditions also imply $\omega^2 - \dot{\omega} = \alpha^2(t) > \rho^2$. Thus, given a CoM height trajectory satisfying $\alpha(t) > \rho$, i.e. $z_{com} - z_{ecmp} > 0$ and $\ddot{z}_{com} > -g$, an admissible ω trajectory can be computed from the natural frequency of the LIPM using reverse-time integration.

Given a desired terminal state, ω_f, we discretize the reverse-time dynamics and integrate backwards in time using a second-order Runge-Kutta method. When tracking the derived time-varying DCM trajectory, the CoM height closely follows the nominal vertical CoM trajectory assuming no large perturbations occur. Fig. 2 shows the planned eCMP, CoM height and natural frequency trajectories corresponding to a footstep plan with increasingly taller steps. The nominal vertical CoM trajectory is defined by piecewise 5$^{\text{th}}$-order polynomials, and the final time-varying natural frequency is initialized to $\omega_f = \alpha(t_f)$.

It should be noted that reverse-time integration can result in discontinuities between consecutive plans, i.e. $\omega(t_0) \neq \omega_0$, due to the lack of initial boundary conditions. In practice, however, this discontinuity is sufficiently small as to not cause noticeable issues when replanning at the onset of each step. This is partially due to the ω dynamics, which ensure $\omega^2(t_0) - \dot{\omega}(t_0) = \omega_0^2 - \dot{\omega}_0$ given continuous eCMP and CoM height reference trajectories.

C. Planning the DCM trajectory

In order to generate the final DCM reference trajectory, we propose a two-part approach consisting of reverse-time integration for long-term planning and Model Predictive Control for short-term planning. Given the desired eCMP and ω trajectories, a corresponding VRP trajectory can be computed from (11). As discussed in Section III, the time-varying DCM dynamics are unstable with respect to the VRP, causing the DCM to diverge with time. However, in reverse-time the VRP acts like an attractor,

$$\dot{\boldsymbol{\xi}}_r = -\left(\omega - \frac{\dot{\omega}}{\omega}\right)\left(\boldsymbol{\xi} - \mathbf{r}_{vrp}(t_r)\right), \qquad \boldsymbol{\xi}(t_f) = \boldsymbol{\xi}_f, \tag{17}$$

where $\dot{\boldsymbol{\xi}}_r = -\dot{\boldsymbol{\xi}}$ is the reverse-time derivative of the DCM.

Using a similar approach to the previous section, we apply reverse-time integration in order to compute a stable DCM trajectory given a desired terminal state $\boldsymbol{\xi}(t_f) = \boldsymbol{\xi}_f$. For the experiments in Section V, the terminal DCM position is chosen to lie above the center of the support polygon during the final double support phase in the preview window.

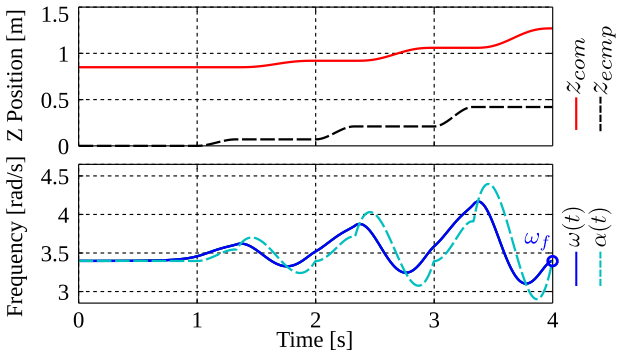

Fig. 2. Top: Reference CoM and eCMP height. Bottom: LIPM and time-varying DCM natural frequency computed using reverse-time integration.

Reverse-time integration of the DCM dynamics results in a discontinuity in the reference trajectory occurring at the beginning of each planning window. Although larger preview windows can be used to minimize the discontinuity, in practice, the initial DCM offset can be significant (> 0.01 m) in the event of step timing and or foothold positioning errors. This can result in significant ZMP errors during transition periods. In order to enforce initial boundary conditions on the DCM state, we implement discrete-time Model Predictive Control (MPC) over a short preview window occurring at the beginning of each time horizon. The Model Predictive Controller drives the DCM state to the reference trajectory computed via reverse-time integration in a smooth manner.

In order to compute the MPC solution, we first define the discrete-time DCM dynamics along a single axis,

$$\begin{aligned} \begin{bmatrix} \xi_{k+1} \\ \dot{\xi}_{k+1} \end{bmatrix} &= \underbrace{\begin{bmatrix} 1 & \Delta t \\ 0 & 1 \end{bmatrix}}_{\mathbf{A}} \begin{bmatrix} \xi_k \\ \dot{\xi}_k \end{bmatrix} + \underbrace{\begin{bmatrix} \Delta t^2/2 \\ \Delta t \end{bmatrix}}_{\mathbf{B}} u_k \\ y_k &= \underbrace{\begin{bmatrix} 1 & -\omega_k/(\omega_k^2 - \dot{\omega}_k) \end{bmatrix}}_{\mathbf{C}_k} \begin{bmatrix} \xi_k \\ \dot{\xi}_k \end{bmatrix}. \end{aligned} \tag{18}$$

Here Δt represents the sample period, ξ_k and $\dot{\xi}_k$ represent the DCM position and velocity, u_k represents the DCM acceleration, and y_k represents the VRP at time step k. Given an N-step preview window, the discrete-time DCM trajectory, $\mathbf{v}_\xi \in \mathbb{R}^{2N}$, can be expressed in terms of the initial state, $\boldsymbol{\xi}_0 \in \mathbb{R}^2$, and input trajectory $\mathbf{v}_u \in \mathbb{R}^N$ using the recursive relationship,

$$\mathbf{v}_\xi = \underbrace{\begin{bmatrix} \mathbf{A} \\ \mathbf{A}^2 \\ \vdots \\ \mathbf{A}^N \end{bmatrix}}_{\boldsymbol{\Phi}_0^\xi} \boldsymbol{\xi}_0 + \underbrace{\begin{bmatrix} \mathbf{B} & \mathbf{0} & \dots & \mathbf{0} \\ \mathbf{AB} & \mathbf{B} & \dots & \mathbf{0} \\ \vdots & \vdots & \ddots & \vdots \\ \mathbf{A}^{N-1}\mathbf{B} & \mathbf{A}^{N-2}\mathbf{B} & \dots & \mathbf{B} \end{bmatrix}}_{\boldsymbol{\Phi}_u^\xi} \mathbf{v}_u.$$

Similarly, the VRP output trajectory, $\mathbf{v}_y \in \mathbb{R}^N$, is given by

$$\mathbf{v}_y = \underbrace{\begin{bmatrix} \mathbf{C}_1\mathbf{A} \\ \mathbf{C}_2\mathbf{A}^2 \\ \vdots \\ \mathbf{C}_N\mathbf{A}^N \end{bmatrix}}_{\boldsymbol{\Phi}_0^y} \boldsymbol{\xi}_0 + \underbrace{\begin{bmatrix} \mathbf{C}_1\mathbf{B} & \mathbf{0} & \dots & \mathbf{0} \\ \mathbf{C}_2\mathbf{AB} & \mathbf{C}_2\mathbf{B} & \dots & \mathbf{0} \\ \vdots & \vdots & \ddots & \vdots \\ \mathbf{C}_N\mathbf{A}^{N-1}\mathbf{B} & \mathbf{C}_N\mathbf{A}^{N-2}\mathbf{B} & \dots & \mathbf{C}_N\mathbf{B} \end{bmatrix}}_{\boldsymbol{\Phi}_u^y} \mathbf{v}_u.$$

By expressing the state and output histories in terms of the input trajectory and initial state, the MPC problem can be formulated as a quadratic program (QP) with the elements of $\mathbf{v}_u$ as the decision variables. This approach is inspired by the work of Wieber and Krause who proposed similar MPC approaches for the CoM and CP dynamics [3] [17].

The MPC optimization is formulated as

$$\min_{\mathbf{v}_u} \frac{1}{2}\Delta\mathbf{v}_y^T\mathbf{Q}\Delta\mathbf{v}_y + \frac{1}{2}\mathbf{v}_u^T\mathbf{R}\mathbf{v}_u + \frac{1}{2}\Delta\mathbf{v}_\xi^T\mathbf{F}\Delta\mathbf{v}_\xi, \qquad (19)$$

where $\Delta\mathbf{v}_y = \mathbf{v}_y - \mathbf{v}_{y,s}$ and $\Delta\mathbf{v}_\xi = \mathbf{v}_\xi - \mathbf{v}_{\xi,s}$ represent the output and state error vectors given the VRP and DCM solution trajectories, $\mathbf{v}_{y,s}$ and $\mathbf{v}_{\xi,s}$, obtained via reverse-time integration. Here $\mathbf{Q}$ and $\mathbf{F}$ are positive-semidefinite cost matrices weighting the VRP and DCM error terms. The third cost matrix, $\mathbf{R} > 0$, penalizes the DCM acceleration, thereby smoothing the optimized trajectories.

The unconstrained QP (19) is a variant of the linear-quadratic regulator (LQR) and can be solved using the least squares formulation, $\mathbf{b}_u = \mathbf{A}_u\mathbf{v}_u$ given

$$\mathbf{b}_u = -\mathbf{Q}\boldsymbol{\Phi}_u^{y\,T}(\boldsymbol{\Phi}_0^y\boldsymbol{\xi}_0 - \mathbf{v}_{y,s}) - \mathbf{F}\boldsymbol{\Phi}_u^{\xi\,T}(\boldsymbol{\Phi}_0^\xi\boldsymbol{\xi}_0 - \mathbf{v}_{\xi,s})$$

$$\mathbf{A}_u = \boldsymbol{\Phi}_u^{y\,T}\mathbf{Q}\boldsymbol{\Phi}_u^y + \boldsymbol{\Phi}_u^{\xi\,T}\mathbf{F}\boldsymbol{\Phi}_u^\xi + \mathbf{R}.$$

Noting that $\mathbf{A}_u$ is a positive-definite symmetric matrix, the solution can be computed efficiently using Cholesky decomposition. In order to compute the three-dimensional MPC solution over the desired preview window, we solve separate QPs for the x, y and z trajectories.

Fig. 3 shows the optimized DCM and VRP trajectories in the lateral plane for a 2-step plan. Reverse time-integration is used to compute reference trajectories over a 2 s horizon. The MPC solution is computed over the first 0.5 s with $N = 100$, $\mathbf{Q} = \boldsymbol{I}$, $\mathbf{R} = 10^{-4}\boldsymbol{I}$, and $\mathbf{F} = 10^6\mathbf{S}_N$ where $\mathbf{S}_N$ is a selection matrix designed to weight only the final value of $\Delta\mathbf{v}_\xi$. The initial DCM velocity is set to 0 m/s to simulate a transition from standing to stepping.

D. Tracking the DCM trajectory

The time-varying DCM trajectory is updated at the beginning of each double support phase and tracked using the following control law,

$$\mathbf{r}_{vrp} = \boldsymbol{\xi} - \frac{1}{\omega - \frac{\dot{\omega}}{\omega}}\left(\dot{\boldsymbol{\xi}}_r + \mathbf{k}_\xi(\boldsymbol{\xi}_r - \boldsymbol{\xi}) + \mathbf{k}_\Xi\int(\boldsymbol{\xi}_r - \boldsymbol{\xi})\,dt\right),$$

where $\boldsymbol{\xi}_r$ and $\dot{\boldsymbol{\xi}}_r$ are the reference DCM position and velocity and k_ξ and k_Ξ are non-negative feedback gains. The first term cancels the nominal DCM dynamics, and the second term implements a proportional-integral controller with unity feedforward. Given the commanded VRP setpoint and CoM estimate, we compute the desired linear momentum rate of change using $\dot{\boldsymbol{l}}_d = m\left(\omega^2 - \dot{\omega}\right)(\mathbf{x} - \mathbf{r}_{vrp})$ based on the VRP definition (9). For the experiments presented in Section V, the momentum rate of change objective is tracked using a model-based whole-body controller similar to [18] and [19].

We note that it is also possible to implement traditional Model Predictive Control by replanning the DCM reference trajectory at each time step. In this case, the proposed tracking controller is not required, as the desired linear momentum rate of change is computed directly from the reference VRP. Although more computationally intensive, this approach may offer increased robustness to large disturbances and is intended as a future research direction.

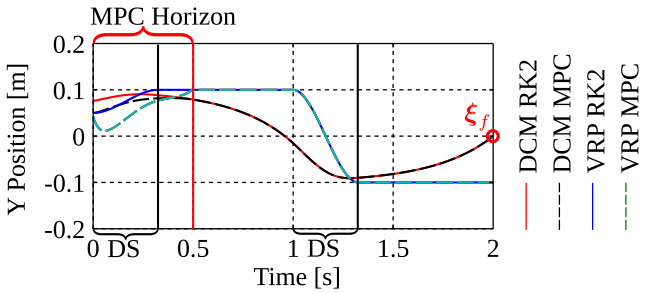

Fig. 3. Lateral DCM and VRP trajectories for a 2-step plan. The DCM RK2 trajectory is computed using reverse time-integration over the 2.0 s time-horizon. The DCM MPC trajectory is computed using linear MPC over a 0.5 s preview window. Double support phases are marked on the x-axis.

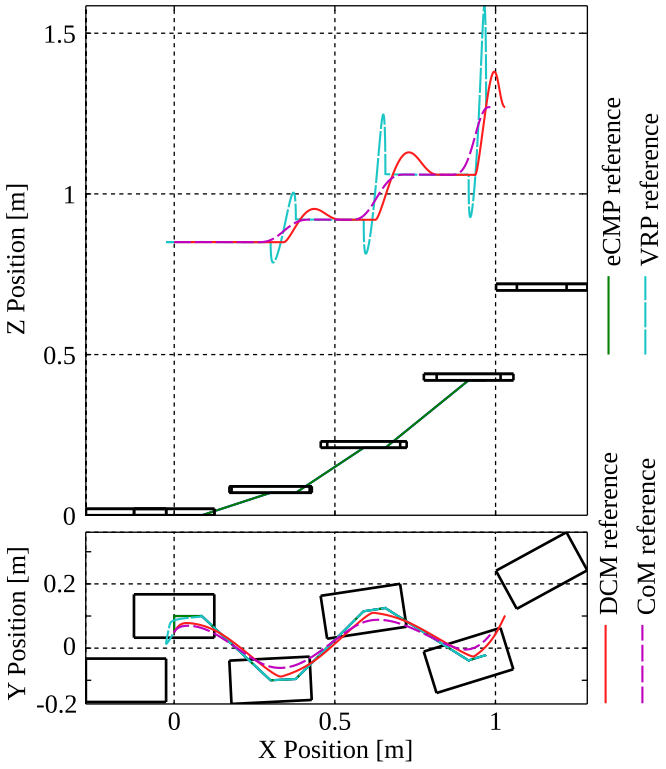

Fig. 4. DCM, CoM, VRP and eCMP plans given a 4-step preview window with increasing step height and turning radius.

V. Results

Fig. 4 shows an example reference trajectory generated using the proposed approach. The desired footstep plan consists of 4 forward steps of increasing height (0.07, 0.14, 0.21 and 0.28 m) with a step duration of 1 s, double support duration of 0.33 s, and single support duration of 0.67 s. The nominal vertical CoM trajectory is constant during each double support phase and increases to a height of 0.85 m

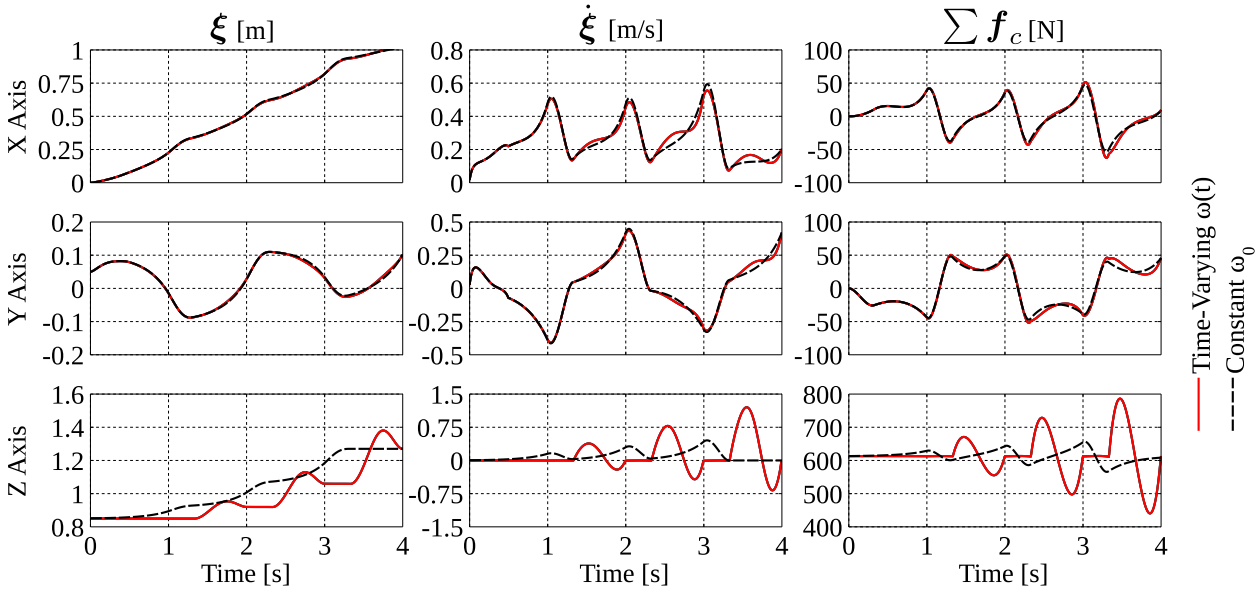

Fig. 5. Comparison of DCM and contact force trajectories for the step plan shown in Fig. 4 given constant and time-varying natural frequencies.

above the support foot during each single support phase. The eCMP, VRP, and DCM trajectories are discretized with a sample period of $\Delta t = 0.005$ s.

Fig. 5 compares the corresponding DCM and contact force trajectories given a constant and time-varying natural frequency (shown in Fig. 2). Note that the vertical DCM trajectories vary significantly due to the natural frequency's effect on the VRP height. Although affected to a lesser degree, the time-varying and time-invariant horizontal DCM trajectories begin to diverge as $\left\|\left(\omega - \frac{\dot{\omega}}{\omega}\right) - \omega_0\right\|$ becomes large. This trend also appears in the commanded contact forces. While the specific normal forces associated with a constant natural frequency may be sub-optimal for stepping over varied terrain due to range of motion or torque limitations, the time-varying DCM dynamics provide a principled approach to planning DCM trajectories with generic normal force profiles. This could enable the design of DCM-based walking trajectories that more closely emulate biological models such as SLIP [20].

The proposed planning and control approach was tested using a 30-DoF model of THOR, the Tactical Hazardous Operations Robot [21], simulated in Gazebo [22]. THOR is a torque-controlled humanoid developed to compete in the DARPA Robotics Challenge. Fig. 6 shows the simulated THOR platform walking over 0.075 and 0.15 m tall cinder blocks, and Fig. 7 shows the resulting DCM and VRP trajectories. The step duration is 1.6 s and the double support duration is 0.32 s. For this experiment, the DCM plan was computed at the beginning of each double support phase given a 3-step preview window. As seen in Fig. 7, the robot is able to track the time-varying DCM reference trajectory with minimal deviations to the nominal VRP reference using the DCM feedback controller presented in Section IV-D. Here the controller gains were set to $k_\xi = 2.0$ and $k_\Xi = 0.3$.

The step controller updates at 200 Hz real-time on a

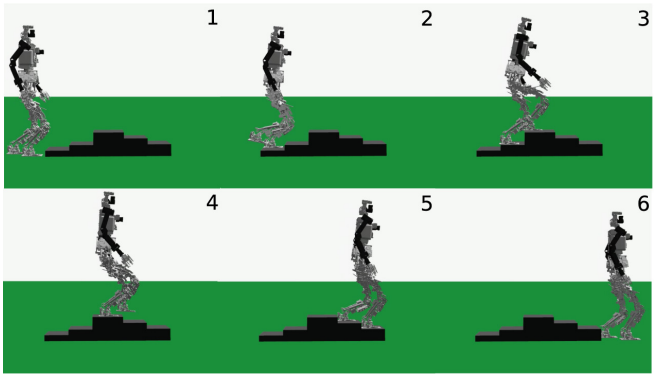

Fig. 6. THOR walking over cinder blocks of varying height in simulation.

3.7 GHz i7 processor. The current unoptimized dynamic planning implementation takes approximately 0.002 s to compute a DCM reference trajectory over a 6.0 s time horizon with a 0.5 s MPC preview window and a 0.005 s sample period. The walking behavior is implemented using a simple state machine to transition between double and single support phases. Admissible joint torque setpoints are computed using a QP-based whole-body controller given the desired end-effector accelerations, momentum rates of change, and frictional contact constraints. In order to mitigate the effects of sensor noise, Kalman filtering is applied to the joint-space velocity measurements, and the DCM position is computed from the estimated joint states using a 36-DoF floating-base model of the robot.

VI. Conclusion

We presented a novel time-varying extension to the DCM and showed that this framework could be used to plan and track DCM reference trajectories with desired ZMP and CoM height characteristics. The time-varying natural frequency

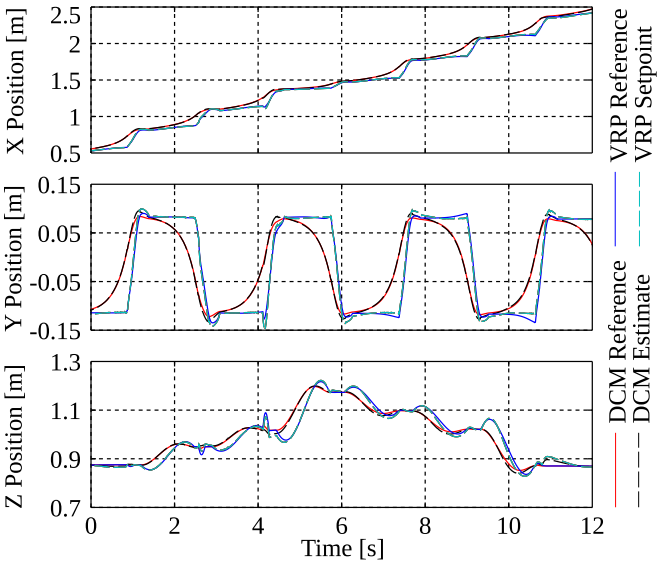

Fig. 7. Estimated and desired DCM and VRP trajectories while walking over cinder blocks in simulation (see Fig. 6). Each step is approximately 1.6 s with a double support duration of 0.32 s.

of the DCM effects the ground reaction forces commanded during stepping and may allow the design of more robust locomotion behaviors on uneven terrain. Although we presented a three-dimensional DCM tracking controller to stabilize the planned trajectories, the proposed approach could also be used for horizontal CP tracking in conjunction with a high-gain CoM height controller. By incorporating reverse-time integration for long-term planning and Model Predictive Control for short-term planning, we are able to achieve real-time performance over a relatively large preview window.

The proposed approach is currently being ported to the THOR hardware platform. Future work will focus on improving the time-varying DCM tracking controller to account for phase delay in the VRP feedback and unmodeled dynamics. We are also investigating full MPC and time-varying LQR approaches for continuous replanning at each time step to simplify adaptive behaviors such as dynamic footstep placement.

Acknowledgments

This work was supported by ONR through grant N00014-11-1-0074 and by DARPA through grant N65236-12-1-1002.

References

[1] S. Kajita, F. Kanehiro, K. Kaneko, K. Yokoi, and H. Hirukawa, "The 3d linear inverted pendulum mode: a simple modeling for a biped walking pattern generation," in *IEEE/RSJ International Conference on Intelligent Robots and Systems*, vol. 1, 2001, pp. 239–246 vol.1.

[2] S. Kajita, F. Kanehiro, K. Kaneko, K. Fujiwara, K. Harada, K. Yokoi, and H. Hirukawa, "Biped walking pattern generation by using preview control of zero-moment point," in *IEEE International Conference on Robotics and Automation*, vol. 2, 2003, pp. 1620–1626 vol.2.

[3] P.-B. Wieber, "Trajectory free linear model predictive control for stable walking in the presence of strong perturbations," in *IEEE-RAS International Conference on Humanoid Robots*, Genova, Italie, 2006.

[4] J. Park and Y. Youm, "General zmp preview control for bipedal walking," in *Robotics and Automation, 2007 IEEE International Conference on*, April 2007, pp. 2682–2687.

[5] S. Kuindersma, F. Permenter, and R. Tedrake, "An efficiently solvable quadratic program for stabilizing dynamic locomotion," in *In Proceedings of the International Conference on Robotics and Automation*, May 2014.

[6] J. Pratt, J. Carff, S. Drakunov, and A. Goswami, "Capture point: A step toward humanoid push recovery," in *Humanoid Robots, 2006 6th IEEE-RAS International Conference on*, Dec 2006, pp. 200–207.

[7] T. Takenaka, T. Matsumoto, and T. Yoshiike, "Real time motion generation and control for biped robot -1st report: Walking gait pattern generation-," in *Intelligent Robots and Systems, 2009. IROS 2009. IEEE/RSJ International Conference on*, Oct 2009, pp. 1084–1091.

[8] J. Englsberger, C. Ott, M. Roa, A. Albu-Schaffer, and G. Hirzinger, "Bipedal walking control based on capture point dynamics," in *Intelligent Robots and Systems (IROS), 2011 IEEE/RSJ International Conference on*, Sept 2011, pp. 4420–4427.

[9] J. Englsberger, C. Ott, and A. Albu-Schaffer, "Three-dimensional bipedal walking control using divergent component of motion," in *Intelligent Robots and Systems (IROS), 2013 IEEE/RSJ International Conference on*, Nov 2013, pp. 2600–2607.

[10] M. Morisawa, S. Kajita, F. Kanehiro, K. Kaneko, K. Miura, and K. Yokoi, "Balance control based on capture point error compensation for biped walking on uneven terrain," in *Humanoid Robots (Humanoids), 2012 12th IEEE-RAS International Conference on*, Nov 2012, pp. 734–740.

[11] J. Englsberger and C. Ott, "Integration of vertical com motion and angular momentum in an extended capture point tracking controller for bipedal walking," in *Humanoid Robots (Humanoids), 2012 12th IEEE-RAS International Conference on*, Nov 2012, pp. 183–189.

[12] M. B. Popovic and H. Herr, "Ground reference points in legged locomotion: Definitions, biological trajectories and control implications," *Int. J. Robot. Res*, vol. 24, 2005.

[13] T. Koolen, T. De Boer, J. Rebula, A. Goswami, and J. Pratt, "Capturability-based analysis and control of legged locomotion, part 1: Theory and application to three simple gait models," *Int. J. Rob. Res.*, vol. 31, no. 9, pp. 1094–1113, Aug. 2012.

[14] T. Sugihara, "Standing stabilizability and stepping maneuver in planar bipedalism based on the best com-zmp regulator," in *Robotics and Automation, 2009. ICRA '09. IEEE International Conference on*, May 2009, pp. 1966–1971.

[15] J. Englsberger, T. Koolen, S. Betrand, J. Pratt, C. Ott, and A. Albu-Schaffer, "Trajectory generation for continuous leg forces during double support and heel-to-toe shift based on divergent component of motion," in *Intelligent Robots and Systems (IROS), 2014 IEEE/RSJ International Conference on*, Sept. 2014.

[16] P. Sardain and G. Bessonnet, "Forces acting on a biped robot. center of pressure-zero moment point," *Systems, Man and Cybernetics, Part A: Systems and Humans, IEEE Transactions on*, vol. 34, no. 5, pp. 630–637, Sept. 2004.

[17] M. Krause, J. Englsberger, P.-B. Wieber, and C. Ott, "Stabilization of the capture point dynamics for bipedal walking based on model predictive control," in *In: proceedings on IFAC conference SYROCO 2012*, 2012.

[18] T. Koolen, J. Smith, G. Thomas, S. Bertrand, J. Carff, N. Mertins, D. Stephen, P. Abeles, J. Englsberger, S. McCrory, J. van Egmond, M. Griffioen, M. Floyd, S. Kobus, N. Manor, S. Alsheikh, D. Duran, L. Bunch, E. Morphis, L. Colasanto, K.-L. Ho Hoang, B. Layton, P. Neuhaus, M. Johnson, and J. Pratt, "Summary of team IHMC's virtual robotics challenge entry," in *Proceedings of the IEEE-RAS International Conference on Humanoid Robots , Atlanta, GA, Oct 2013*.

[19] A. Herzog, L. Righetti, F. Grimminger, P. Pastor, and S. Schaal, "Experiments with a hierarchical inverse dynamics controller on a torque-controlled humanoid," *arXiv preprint arXiv:1305.2042*, 2013.

[20] H. Geyer, A. Seyfarth, and R. Blickhan, "Compliant leg behaviour explains basic dynamics of walking and running," in *Proc Biol Sci.*, Nov. 2006.

[21] B. Lee, "Design of a humanoid robot for disaster response," Master's thesis, Virginia Polytechnic Institute and State University, April 2014.

[22] N. Koenig and A. Howard, "Design and use paradigms for gazebo, an open-source multi-robot simulator," in *Intelligent Robots and Systems, 2004. (IROS 2004). Proceedings. 2004 IEEE/RSJ International Conference on*, vol. 3, Sept 2004, pp. 2149–2154 vol.3.